HHS Public Access

Author manuscript

Opt Lett. Author manuscript; available in PMC 2016 August 10.

Published in final edited form as:

Opt Lett. 2015 July 1; 40(13): 3201–3204.

Multi-view second-harmonic generation imaging of mouse tail tendon via reflective micro-prisms

Bruce Wen[1,2,3,†], **Kirby R. Campbell**[1,†], **Benjamin L. Cox**[1,2,3], **Kevin W. Eliceiri**[1,2,3], **Richard Superfine**[4], and **Paul J. Campagnola**[1,2,*]

[1]Laboratatory for Optical and Computational Instrumentation, Department of Biomedical Engineering, University of Wisconsin—Madison, 1550 Engineering Drive, Madison, Wisconsin 53706, USA

[2]Medical Physics Department, University of Wisconsin—Madison, Highland Avenue, Madison, Wisconsin 53706, USA

[3]Morgridge Institute for Research, 330 N. Orchard Street, Madison, Wisconsin 53715, USA

[4]Departments of Physics and Astronomy, University of North Carolina, Chapel Hill, North Carolina 27599, USA

Abstract

Here we experimentally show that second-harmonic generation (SHG) imaging is not sensitive to collagen fibers oriented parallel to the direction of laser propagation and, as a consequence, can potentially miss important structural information. As an alternative approach, we demonstrate the use of reflective micro-prisms to enable multi-view SHG imaging of mouse tail tendon by redirecting the focused excitation and collection of subsequent emission. Our approach data corroborates the theoretical treatment on vanishing and nonvanishing orientations, where fibers along the laser direction are largely transparent by SHG. In strong contrast, the two-photon excited fluorescence of dye-labeled collagen fibers is isotropic and is not subject to this constraint. We utilized Pearson correlation to quantify differences in fluorescent and backward detected SHG images of the tendon fiber structure, where the SHG and TPEF were highly statistically correlated (0.6–0.8) for perpendicular excitation but were uncorrelated for excitation parallel to the fiber axis. The results suggest that improved imaging of 3D collagen structure is possible with multi-view SHG microscopy.

Second-harmonic generation (SHG) imaging has emerged as a powerful modality for visualizing the collagen assembly in a wide range of normal and diseased tissue types [1,2]. Applications for imaging structural changes in many pathologic conditions, including cancers [3–5], fibroses [6,7], and connective tissue disorders [8] have received considerable attention, as changes in the collagen rich extracellular matrix (ECM) are often revealed by SHG imaging via changes in fibrillar morphology, intensity, and polarization properties. A limiting aspect of SHG imaging is that it is not a true 3D technique. Specifically, while 3D data is built up from stacking a series of 2D *en face* images, due to the electric dipole

*Corresponding author: pcampagnola@wisc.edu.
†These authors contributed equally to this work.

interaction, fully axially oriented fibers (i.e., along the laser direction) are transparent. This phenomenon is not commonly seen in fluorescence imaging as probe molecules (either dyes or fluorescent proteins) typically have rotational freedom, and absorb at all angles. The most notable exception is imaging of membrane staining dyes (e.g., DiI or ANEPPS), where a "ring stain" is often observed due to the rotational constraints of the dye molecules being bound in the membrane. The endogenous SHG contrast from collagen molecules within fibrils has these same constraints. This situation results in a loss of information in determining the structure of 3D ECM.

A solution to this problem is to acquire SHG images from different directions of the excitation laser relative to the fixed specimen. We note that this is distinct from probing different structural aspects via performing polarization analysis from the same direction of laser propagation [9]. Here we demonstrate SHG microscopy in conjunction with reflective micro-prisms to image the collagen fiber structure in mouse tail tendon from multiple vantage points to tailor true 3D visualization of the collagen fibers within a matrix. Such prisms have previously been used for several other applications [10–13]. Here we utilize the micro-prisms to excite and collect the backward directed SHG from different views. Backward detected SHG is comprised of a mixture of the emitted signal and subsequent scattering at the SHG wavelength. In tendon, the emitted directionality, which we have denoted F_{SHG}/B_{SHG}, is ~7:1 [14,15], but given the strength of the absolute intensity, this is more than sufficient for imaging.

Collagen I fibers consist of a complex hierarchal assembly, as shown in Fig. 1 First, individual triple helical collagen molecules are covalently linked to into fibrils with diameters ranging from 20 to 200 nm, depending on the tissue. Fibrils are further organized into fibers, where the latter are the quantity visualized in the SHG microscope. Additionally, fibers can crimp, causing the components of the bundle to appear offset from the long axis.

The induced polarization of a medium subjected to an intense electromagnetic field can be related in a power series of the field strength E_i (i, j, k are Cartesian components) by the expression

$$P_i = \varepsilon_0 \chi_{ij}^{(1)} E_j + \varepsilon_0 \chi_{ijk}^{(2)} E_j E_k + \varepsilon_0 \chi_{ijkl}^{(3)} E_j E_k E_{l+\ldots}, \quad (1)$$

where P_i is the ith component of the induced polarization, and ε_0 is the vacuum permittivity, $\chi_{ij}^{(n)}$ denotes the nth order susceptibility and is a tensor of rank corresponding to the number of subscripts. For example, $\chi_{ijk}^{(2)}$ can be expressed by the third-rank d-tensor given by $d_{ijk} = \chi_{ijk}^{(2)}/2$, and the effective d-value is written as $d_{\text{eff}} = \hat{\mathbf{e}} d$, where $\hat{e}$ is a unit vector describing the electric field or polarization field of the light wave. The tensor related to SHG, $\chi^{(2)}$, reflects the symmetry and nonlinear optical properties of the material and is the quantity visualized in the microscope.

For the cylindrical structure of collagen fibrils (C_∞ symmetry), the most general vector expression for the polarization dependence of SHG is [16]

$$d_{\text{eff}}=(\hat{e}_1,\hat{e}_2,\hat{e}_3)\begin{bmatrix}0&0&0&0&0&d_{16}\\d_{21}&d_{22}&d_{23}&0&0&0\\0&0&0&d_{34}&0&0\end{bmatrix}\begin{bmatrix}\hat{e}_1^2\\\hat{e}_2^2\\\hat{e}_3^2\\2\hat{e}_2\hat{e}_3\\2\hat{e}_3\hat{e}_1\\2\hat{e}_1\hat{e}_2\end{bmatrix}, \quad (2)$$

where the coordinate system of the laser electric field or the polarization field of the light wave is related to the collagen fiber by the unit vectors $\hat{e}_1$, $\hat{e}_2$, and $\hat{e}_3$.

In accordance with previous approaches [17], collagen fibrils are assumed to have C_∞ mm symmetry ($x = z$) along the fiber axis (the y-axis in Fig. 1) as this simplifies the treatment relative to the exact C_3v. Cylindrical symmetry ($x = z$) implies that $d_{16} = d_{34}$ and $d_{21} = d_{23}$ and Kleinman symmetry gives $d_{16} = d_{21}$. Therefore, we can assume $d = d_{16} = d_{34} = d_{21} = d_{23}$ For circular polarization (as commonly used) [9], the electric field of the laser along the collagen fiber can be described by

$$(\hat{e}_1,\hat{e}_2,\hat{e}_3)=(\sin(\omega t),0,\cos(\omega t)). \quad (3)$$

After inserting $\hat{\mathbf{e}}$, Eq. (2) becomes

$$d_{\text{eff}}=2d_{16}\sin^2(\omega t)\hat{e}_2, \quad (4)$$

since here $\hat{e}_2 = \varnothing$, $d_{\text{eff}} = \varnothing$, it is seen that there will not be any SHG emission in this case. This is rigorously true only if all of the dipole moments align exactly along the direction of the fiber axis. However, a previous study suggested that the collagen molecules may have a small tilt angle with respect to the fibril axis [18], where in this more realistic scenario, the SHG will be greatly diminished but not completely extinguished. By contrast, if the excitation laser propagates along the z axis as [sin(ω*t), cos(ω*t), 0], the following expression would apply:

$$d_{\text{eff}}=[d_{22}\cos^2(\omega t)\hat{e}_2+2d\ \sin^2(\omega t)]\ \cos(\omega t)\mathbf{y}. \quad (5)$$

(Here **y** is the unit vector in *y* direction) in which case only *y* axis polarization components will result in nonvanishing SHG emission. We note that there will be a small axial contribution at high NA (~ > 1.0) due to polarization scrambling (unpublished results).

We can experimentally verify these suppositions and take steps toward 3D imaging by imaging mouse tail tendon from different orthogonal views. Tendon is ideal for this purpose due to the regularity of the fibril/fiber structure. In this experiment, we arrange two 1-mm micro-prisms (Precision Optical, Costa Mesa, California) at orthogonal vantage points of the tendon. One micro-prism is placed facing the end (end view) of the mouse tail tendon, and

one is placed on the side (side view) as shown in Fig. 2. The excitation beam path changes direction on the mirrored face of the prism and propagates into different sides of the tendon. Using a 40× 0.8-NA water immersion lens (Olympus), we achieved a penetration depth of about 160 um on both the side and end views. Images are collected in the backward SHG geometry. The full 0.8-NA is retained at this thickness.

We placed the mouse tail tendon in both a straight and bent (u-shape) configuration in front of the prisms as shown in Fig. 2. The tendon was wet mounted in PBS using a chamber with a silicon spacer and carefully sealed with nail polish to avoid evaporation. Double-sided tape was used to secure the tendon to the glass slide. To afford comparison with fluorescence, the tendon was stained with the dye eosin-y (labels proteins) for 40 min, and rinsed with DI water. Using 890-nm excitation, we sequentially acquired two-photon excited fluorescence (TPEF) and SHG images with a 620-nm/90-nm filter and 445-nm/20-nm bandpass filter (Semrock, Rochester, New York), respectively.

SHG and two-photon fluorescent images of stained mouse tail tendon are acquired using excitation and collection from multiple orientations, where in each case the collection is in the epi-direction of the excitation. The fluorescence from the eosin dye acts as a control relative to the SHG. This is because as the dye binds nonspecifically to collagen fibers and will have an overall isotropic distribution and should be observed from all orientations. The SHG and TPEF comparison is obtained for two cases, where the tendon is left straight [Fig. 2(b)] and also for the case where it is bent into a u-shape near the surface of the end view prism [Fig. 2(c)]. Based on Eqs. (4) and (5), quantifiable differences in the SHG emission should result when exciting the tendon from different angles for fibers oriented parallel and perpendicular to the laser direction.

As shown in Fig. 3, the bent u-shaped mouse tail tendon configuration yields similar results by both SHG (row 2) and TPEF (row 1) for the end (column a) and side (column b) views. These results are indeed all consistent with Eqs. (4) and (5). Note that some regions of the crimp (top and bottom) lack SHG contrast but are seen by TPEF. This is because these fibers are oriented parallel to the laser propagation, and the SHG should vanish. This effect with tendon has been shown previously [19].

The side view images for the straight tendon remain similar (column c). However, this configuration shows highly significant differences in the SHG (row 2) and TPEF (row 1) end view images (column d). Fiber and fiber bundles sticking out of the focus plane and also the tip of the tendon where it was initially cut can be clearly observed in the fluorescence images. As predicted by Eq. (4), there is essentially no SHG contrast from these fibers as they are aligned parallel to the excitation laser beam (see Fig. 1) where only the boundary of each fiber bundle can be discerned with much lower comparative intensity. Furthermore, when examining axial sections through the fiber, this low signal quickly vanishes away from the boundary and may be the result of the cutting process. These results qualitatively agree with theoretical predictions of the diminished SHG emission when the fibers align with the propagation direction of the excitation laser.

Correlation analysis was used to statistically evaluate the similarity of TPEF and SHG images on a pixel-by-pixel basis for different views of the tendon fibers. The Pearson coefficient was determined over the entire 100–160 μm stacks in 1-μm step sizes of the two imaging modalities for both the side and end views. When the two image stacks are perfectly similar, the Pearson coefficient is 1.0 and becomes 0.0 when no correlation exists.

For the u-shaped mouse tail tendon orientation, the obtained Pearson coefficients (after thresholding) for the front and side views were 0.77 and 0.81, respectively, and are statistically correlated. Note that complete correlation is not expected due to the crimped regions, where fluorescence will occur, but SHG will be largely extinguished as these fibers will be parallel to the laser propagation. For the straight tendon arrangement, the Pearson coefficient is 0.60 from the side view but decreased significantly to −0.08 indicating very little correlation between the TPEF and SHG image stacks. To view these correlations (and lack thereof) graphically, Row 3 of Fig. 3 shows the overlap of the grayscale intensity histograms of the respective SHG and TPEF distributions, where for perfect correlation, all points would fall on the diagonal. The observed greatly diminished SHG intensity and lack of correlation with the TPEF for the end view of the straight tendon configuration agrees with the theoretical prediction that little SHG emission will result from fibers that lie parallel to the direction of laser propagation.

While the emission angles for SHG from tissues are not known as they are not perfectly phase-matched, based on phase-matching arguments, little SHG is expected in the orthogonal direction to the excitation [20]. Moreover, scattering from the orthogonal direction will be minimal, as the high scattering anisotropy of tendon (~0.95) leads to essentially all forward directed scatter [14]. Thus the SHG collected in the backward direction from the reflective prism is highly similar to that of *en face* imaging. We note that it is possible to achieve this result through tilting the specimen relative to the laser direction, and obtaining multiple views through two micro-prisms is superior due to design considerations. We also point out that working distance considerations preclude simultaneous side/end view prism viewing and normal *en face* imaging.

In summary, by comparing fluorescence and SHG images, we demonstrate some of the limitations of the SHG method for true 3D imaging of collagen. While we have not presented new theory, validation of these visualization constraints of SHG imaging require the appropriate arrangement for multi-view imaging. This approach can be implemented for a range of SHG investigations. This is important as there is great promise in understanding 3D collagen structure, as the multi-view approach here coupled with directional SHG (forward–backward), and polarization-resolved measurements could reveal new insight in the role of collagen in normal and diseased biological processes.

Acknowledgments

Funding. NSF Directorate for Engineering (ENG) (CBET 1402757); Morgridge Institute; NIH National Institute of Biomedical Imaging and Bioengineering (NIBIB) (5P41EB002025).

We thank Karissa Tilbury, Jeremy Rogers, Jeremy Bredfeldt, and Rock Mackie for helpful conversations.

REFERENCES

1. Campagnola PJ, Dong CY. Laser Photon. Rev. 2011; 5:13.
2. Campagnola P. Anal. Chem. 2011; 83:3224. [PubMed: 21446646]
3. Provenzano PP, Eliceiri KW, Campbell JM, Inman DR, White JG, Keely PJ. BMC Med. 2006; 4:38. [PubMed: 17190588]
4. Cicchi R, Massi D, Sestini S, Carli P, De Giorgi V, Lotti T, Pavone FS. Opt. Express. 2007; 15:10135. [PubMed: 19547362]
5. Brown E, McKee T, diTomaso E, Pluen A, Seed B, Boucher Y, Jain RK. Nat. Med. 2003; 9:796. [PubMed: 12754503]
6. Pena AM, Fabre A, Debarre D, Marchal-Somme J, Crestani B, Martin JL, Beaurepaire E, Schanne-Klein MC. Microsc. Res. Tech. 2007; 70:162. [PubMed: 17177275]
7. Sun W, Chang S, Tai DC, Tan N, Xiao G, Tang H, Yu H, Biomed J. Opt. 2008; 13:064010.
8. Lacomb R, Nadiarnykh O, Campagnola PJ. Biophys. J. 2008; 94:4504. [PubMed: 18281387]
9. Chen X, Nadiarynkh O, Plotnikov S, Campagnola PJ. Nat. Protocol. 2012; 7:654.
10. Hajioul H, Mathon J, Viero Y, Bancaud A. Appl. Phys. Lett. 2011; 98:243701.
11. Lindek S, Stefany T, Stelzer EHK. J. Microsc. 1997; 188:280.
12. Seale KT, Reiserer RS, Markov DA, Ges IA, Wright C, Janetopoulos C, Wikswo JP. J. Microsc. 2008; 232:1. [PubMed: 19017196]
13. Yuan J, Melder RJ, Jain RK, Munn LL. Biotechniques. 2001; 30:388. [PubMed: 11233608]
14. LaComb R, Nadiarnykh O, Carey S, Campagnola PJ. J. Biomed. Opt. 2008; 13:021109. [PubMed: 18465958]
15. Lacomb R, Nadiarnykh O, Townsend SS, Campagnola PJ. Opt. Commun. 2008; 281:1823. [PubMed: 19343083]
16. Erikson A, Ortegren J, Hompland T, de Lange Davies C, Lindgren M. J. Biomed. Opt. 2007; 12:044002. [PubMed: 17867806]
17. Stoller P, Kim B-M, Rubinchik AM, Reiser KM, Da Silva LB. J. Biomed. Opt. 2002; 7:205. [PubMed: 11966305]
18. Tuer AE, Akens MK, Krouglov S, Sandkuijl D, Wilson BC, Whyne CM, Barzda V. Biophys. J. 2012; 103:2093. [PubMed: 23200043]
19. Nadiarnykh O, Plotnikov S, Mohler WA, Kalajzic I, Redford-Badwal D, Campagnola PJ. J. Biomed. Opt. 2007; 12:051805. [PubMed: 17994883]
20. Mertz J, Moreaux L. Opt. Commun. 2001; 196:325.

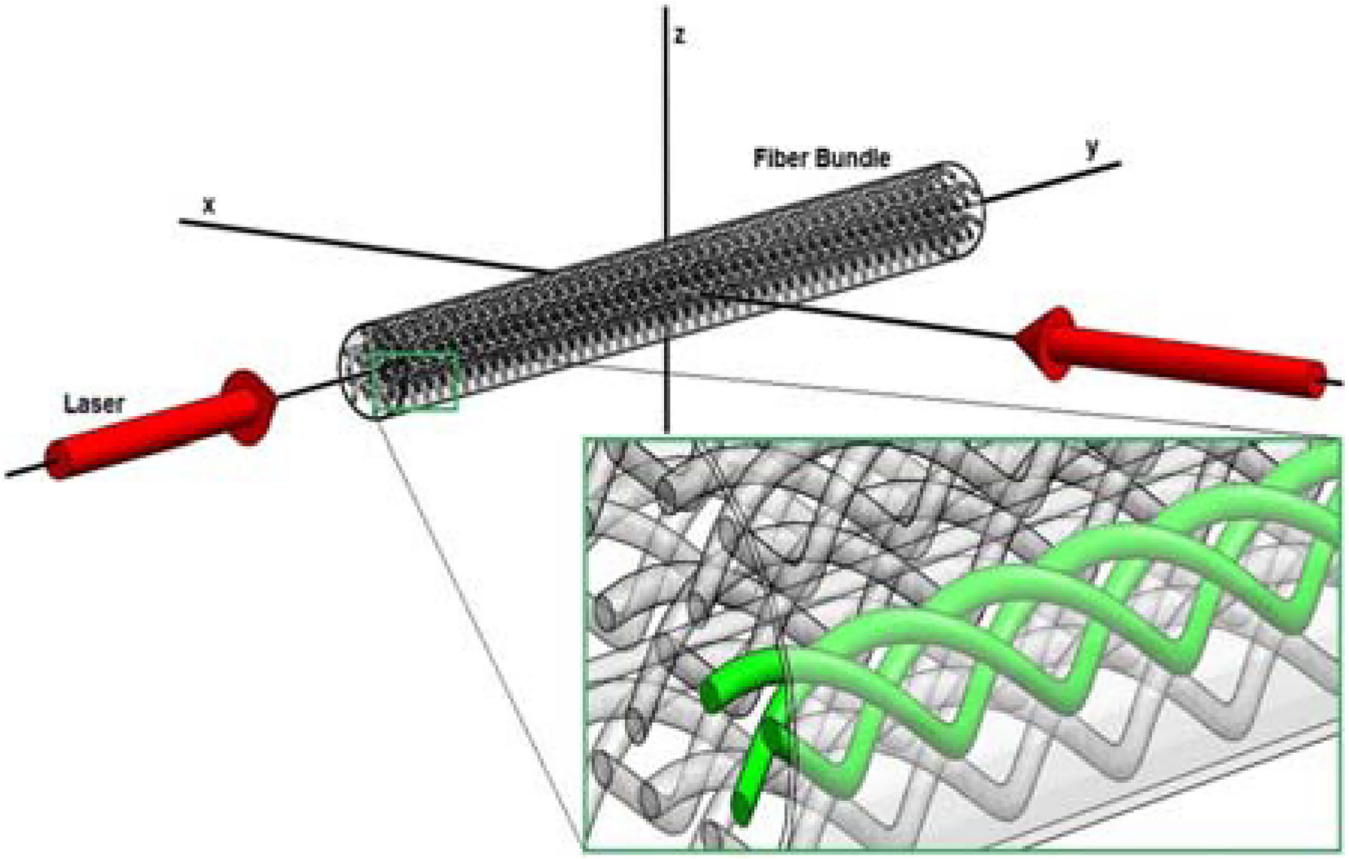

Fig. 1.

End view (*y* axis) and side view (*x* axis) of laser propagation direction relative to the fiber axis (*y* axis)

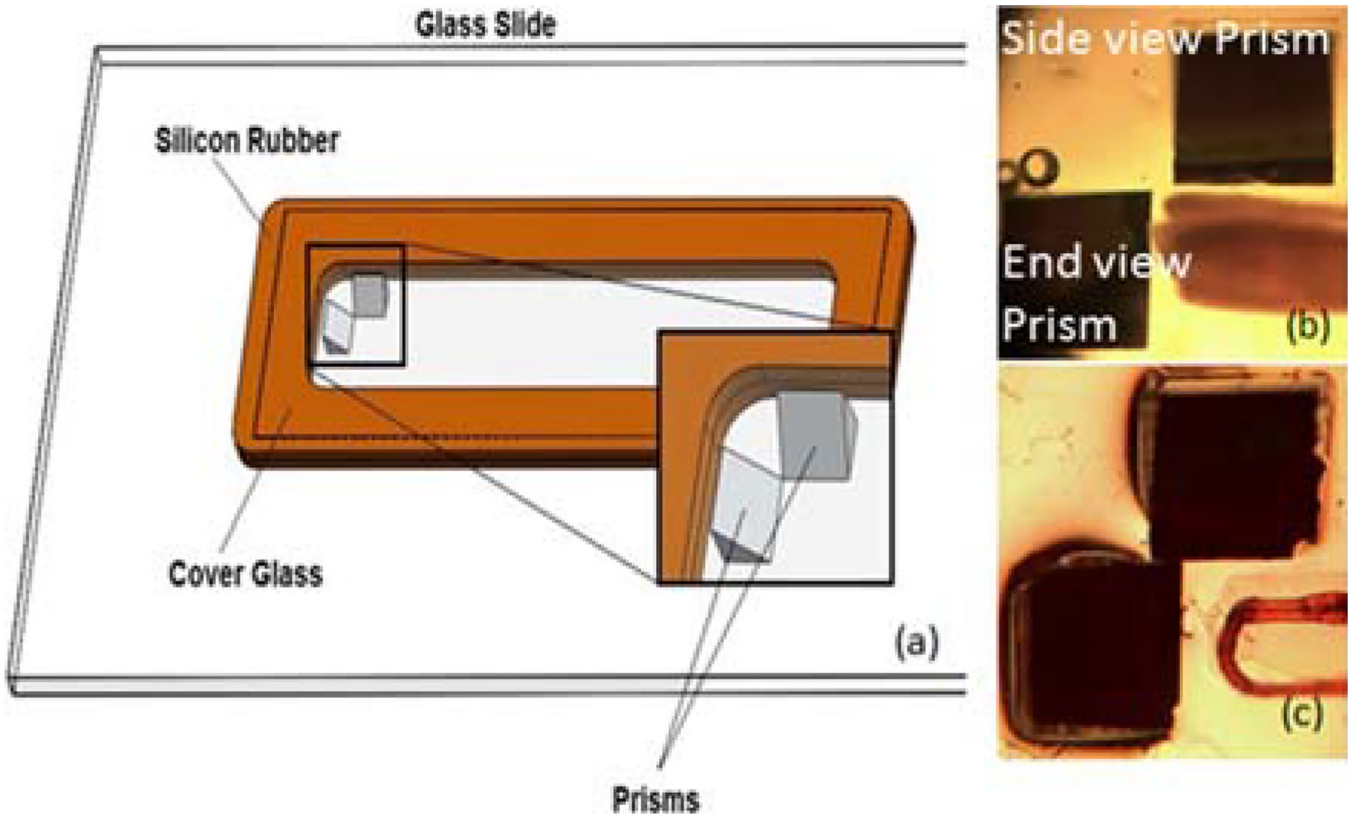

Fig. 2.

(a) Experiment setup showing the layout of the micro-prisms in the chamber, (b) Straight tendon in bright field with a 10× objective, (c) Bent u-shaped tendon in bright field with the same objective.

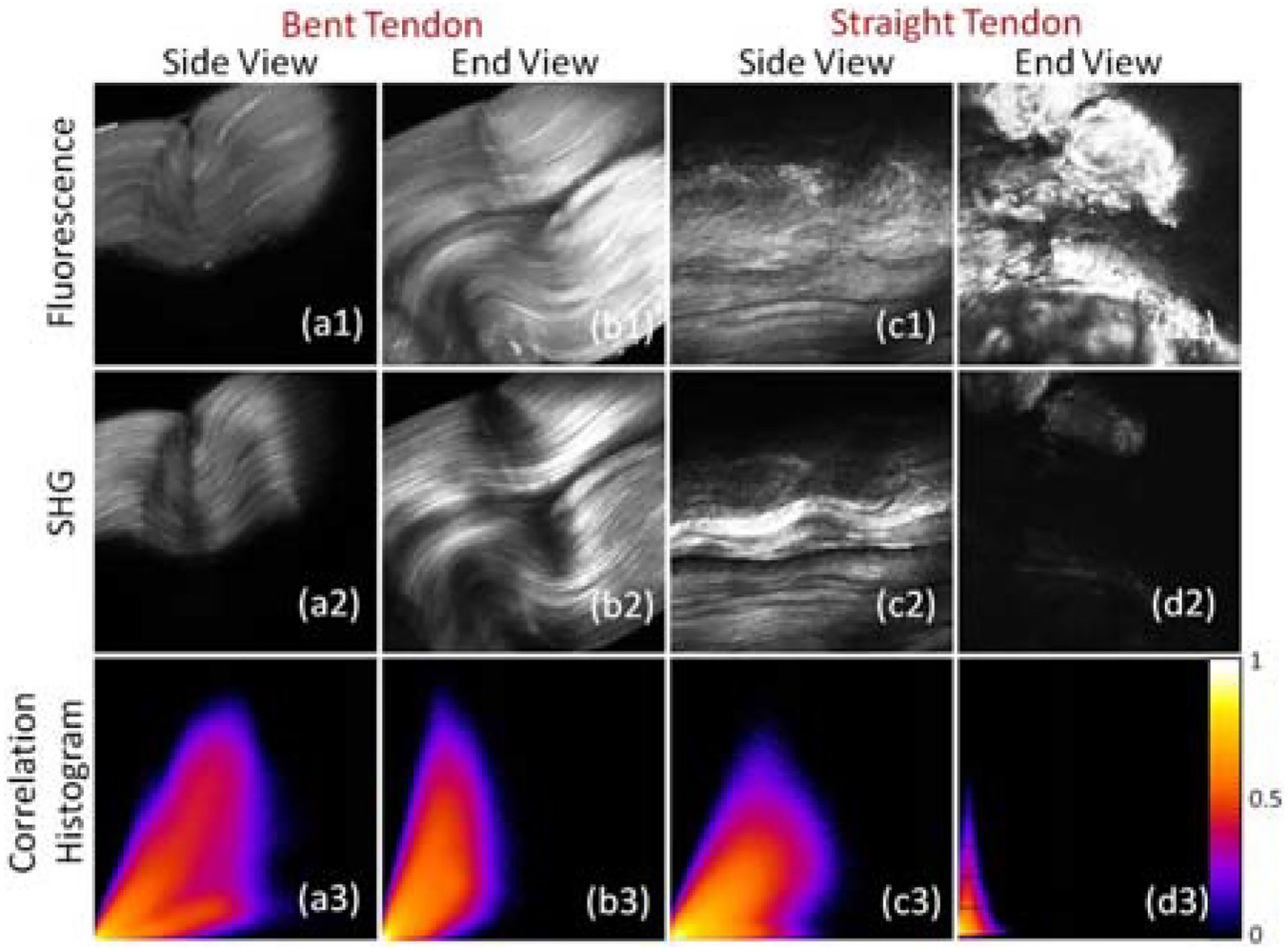

Fig. 3.

Fluorescence image (a1), SHG image (a2), and 2D intensity histogram (a3) for fluorescence and SHG image from side view for bent tendon; fluorescence image (b1), SHG image (b2), and 2D intensity histogram (b3) for fluorescence and SHG image from the end view for bent tendon; fluorescence image (c1), SHG image (c2), and 2D intensity histogram (c3) for fluorescence and SHG image from the side view for straight mouse tendon; fluorescence image (d1), SHG image (d2), and 2D intensity histogram (d3) for fluorescence and SHG image from the end view for straight mouse tendon. The x and y axes for 2D intensity histograms correspond to normalized SHG and TPEF image pixel intensities, respectively. The heatmap is normalized from highest pixel frequency to lowest in 256 color bins. *Field size* = 150 × 150 μ*m*.